Int. J. Electrochem. Sci., 17 **(2022)** Article Number: 221242, doi: 10.20964/2022.12.35

International Journal of
ELECTROCHEMICAL
SCIENCE
www.electrochemsci.org

Synthesis and enhanced visible-light photocatalytic activity of anatase TiO_2/sludge-derived activated carbon composite for degradation of methylene blue

En Shi[1], *Xin Wang*[1], *Miao Zhang*[2,*], *Xinyu Wang*[1], *Jianchun Gao*[2], *Yunbin Zheng*[1], *Xinqiao Zhu*[3,*]

[1] School of Municipal and Environmental Engineering, Shenyang Jianzhu University, Shenyang, 110168, China
[2] School of Material Science and Engineering, Shenyang Jianzhu University, Shenyang, 110168, China
[3] Institute of Nuclear Physics and Chemistry, China Academy of Engineering Physics, Mianyang, 621999, China
[*]E-mail: zhangmiao@sjzu.edu.cn, zhuxinqiao@zju.edu.cn

Received: 28 September 2022 / *Accepted:* 7 November 2022 / *Published:* 30 November 2022

In order to enhance visible-light photocatalytic activity, anatase TiO_2 was modified with sludge-derived activated carbon (SDAC) through the physical mixing and hydrothermal method, respectively. The activated carbon was prepared from sewage sludge by molten salt method. Under visible light irradiation, the removal of methylene blue (MB) with a concentration of 40 mg L^{-1} by TiO_2-SDAC synthesized through the physical mixing and hydrothermal method were up to 70.13% and 95.48%, respectively. Characterization results revealed that a Ti-C bond was formed on the surface of TiO_2-SDAC. Under physical mixing and hydrothermal treatment, carbon atoms can be introduced into the TiO_2 lattice, resulted in tuning the band gap of TiO_2 and extending its optical response to the visible-light region. The photocatalytic degradation of MB was fitted well with Elovich model. It can be concluded that SDAC adsorbs, supports and enhances the photocatalytic activity of TiO_2.

Keywords: Sludge; Activated carbon; Titanium dioxide; Photocatalysis; Methylene blue

1. INTRODUCTION

Sewage sludge, the main byproduct of the wastewater treatment, can cause various environmental problems due to the significant presence of organic, toxic, and heavy metal pollutants [1, 2]. Conventional disposal methods such as landfilling, incineration, and sea dumping are limited in many countries because of the secondary pollutants. One of the most effective methods is to convert sludge into carbon-containing products, which can adsorb and remove organic contaminants from wastewater [3, 4]. Two main methods for preparing activated carbon from sludge include physical and chemical

activation [5]. Compared with the physical activation method, chemical activation technology has the advantages of low activation temperature, short heat treatment time and high carbon yield [6].

Different techniques, including photocatalysis, adsorption, and biological and chemical degradation methods, have employed to treat dye wastewater [7-10]. Photocatalysis is an advanced oxidation process for degrading dyes by utilizing heterogeneous TiO_2 as a photocatalyst [11-13]. The silica, alumina, zeolite, clay and activated carbon are used as supports to improve the photocatalytic efficiency of TiO_2 [14-16]. In the past few years, carbon-supported TiO_2 has received greater attention for its ability to degrade different dyes, such as rhodamine-B (RhB) [17], methyl orange (MO) [18], methylene blue (MB) and reactive red 24 (RR 24) [19]. It is found that the surface properties and the texture of carbon materials have significant influence on the photocatalytic activity of TiO_2 [20].

Activated carbon (AC) is often used with TiO_2 to treat dye wastewater [21, 22]. TiO_2-AC composite synthesized by sol-gel method and hydrothermal process shows high photocatalytic activity in dye degradation tests [23]. By introducing porous carbon, TiO_2 can effectively combine excitation, diffusion and surface transfer of photo-induced carriers to enhance their photocatalytic activity. Some lattice atoms on the TiO_2 surface are replaced by carbon atoms [17]. Therefore, the narrowing of the band gap allows the TiO_2-AC composite to absorb more visible light [24]. Sludge-derived activated carbon (SDAC) has a complex texture structure and surface properties [25, 26]. TiO_2-SDAC prepared by the physical method exhibited higher photocatalytic activity than that of pure TiO_2. The physical mixing method was energy-saving and environment-friendly [27]. However, the photocatalytic activity is low under visible light.

In this study, SDAC is prepared by the molten salt method with $ZnCl_2$ as the activator. Anatase TiO_2 is modified with SDAC through the physical mixing and hydrothermal method with different mass ratios of TiO_2 to SDAC. The adsorption and visible-light photocatalytic degradation of MB are evaluated by kinetic models. The photocatalytic activity of TiO_2-SDAC will be estimated by the degradation of MB under visible light.

2. EXPERIMENTAL

2.1 Materials

The primary raw material for the manufacturing of SDAC was obtained from the secondary sedimentation tank of the Sanboltun Wastewater Treatment Plant in Liaoning Province. The sludge was filtered, dried and passed through a 100-mesh screen for standby. Anatase TiO_2 with the particle size of 40 nm, $ZnCl_2$, and MB were purchased from Shanghai Aladdin Biochemical Technology Co., Ltd., China. Hydrochloric acid and ethanol were purchased from Tianjin Kemiou Chemical Reagent Co., Ltd., China.

2.2 Preparation of sludge-derived activated carbon

SDAC was synthesized by the molten salt method. Equal quality dried sludge and $ZnCl_2$ were weighed and ground evenly, then put into the corundum boat and calcined at 500 ℃ for 2 h in a tubular

furnace. The heating rate of the calcination process was 5°C min^{-1}, and the atmosphere was argon. After calcination, the sample was taken out after cooling to room temperature with the furnace and washed with distilled water and 5% hydrochloric acid solution. After filtration and drying, SDAC was obtained.

2.3 Preparation of TiO_2-sludge-derived activated carbon

TiO_2-SDAC was prepared by two methods, physical mixing and hydrothermal process. For physical mixing, TiO_2 and SDAC were directly added into the reaction system and prepared in situ. The samples were named nTiO_2-SDAC-M, where n represented the mass ratio of TiO_2 to SDAC.

For the hydrothermal process, SDAC was added to 50 ml of TiO_2 aqueous solution. The homogenous mixture was transferred to a 100 mL autoclave reactor and reacted for 4 h at 180°C. After the reaction, the sample was washed with deionized water and dried. Then it was named as nTiO_2-SDAC-H. The optimization details of hydrothermal temperature and time were shown in the supporting materials.

2.4 Characterization

The morphology of the samples was observed by Phenom LE scanning electron microscope (SEM). The magnification was 10000 times, and the acceleration voltage was 10 kV. The functional groups of samples were determined and analyzed by Nicolet iS5 infrared spectrometer, and the test range was from 4000 to 400 cm^{-1}. UV 3600 spectrophotometer was used to determine the spectral absorption properties of the samples. The wavelength range was measured from 200 to 800 nm. An Escalab 250 Xi X-ray photoelectron spectrometer with non-monochromatic Al Kα radiation was used to perform X-ray photoelectron spectroscopy (XPS) spectra. ASAP2020 specific surface area and porosity analyzer from Micromeritics were chosen to determine the adsorption and desorption curve of N_2 at 77.35 K. Specific surface area was calculated by Brunauer-Emmett-Teller (BET) method.

2.5 Photocatalytic degradation experiment

The photocatalytic properties of the samples were tested by using a 500W Xe lamp as a visible light source. The equipment diagram of the photocatalytic degradation experiment was shown in supporting materials (Fig. S1). 100 mg of nTiO_2-SDAC-M placed in a reactor with 300 mL of 40 mg L^{-1} MB solution. At each 30-minute interval, 1.5 mL of solution was taken out and filtered to achieve complete separation of solution and solid. Shanghai Metash UV5500 Spectrophotometer was used to measure the absorbance of MB solution. The adsorption experiment was performed in a dark condition. As a comparative study, the adsorption and photocatalytic degradation properties of nTiO_2-SDAC-H were tested in the same experimental process.

3. RESULTS AND DISCUSSION

3.1 Characterization results

The morphology of the samples was characterized by scanning electron microscopy (Fig. 1). For both 0.4TiO_2-SDAC-M and 0.4TiO_2-SDAC-H, TiO_2 nanoparticles are irregularly shaped, agglomerated and attached to the surface of SDAC [28].

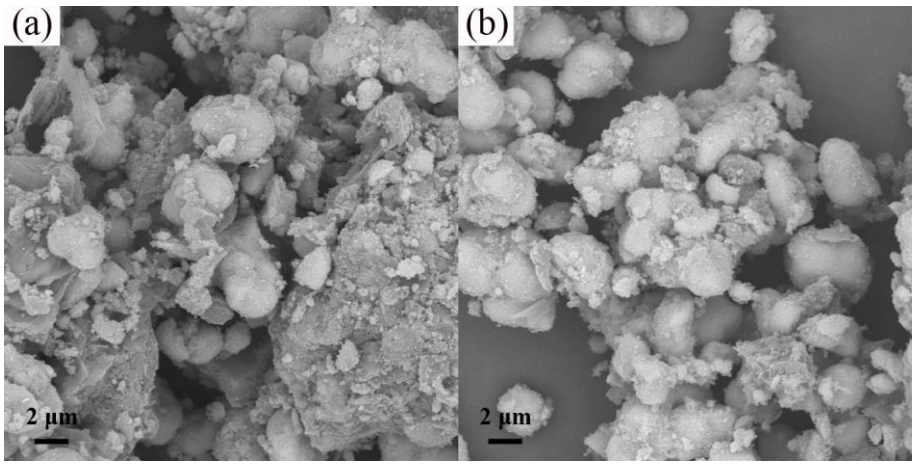

Figure 1. SEM images of (a) composite of 0.4TiO_2-SDAC-M prepared by physical mixing with mass ratio of 0.4 and (b) composite of 0.4TiO_2-SDAC-H prepared by hydrothermal process for 4 h at 180°C.

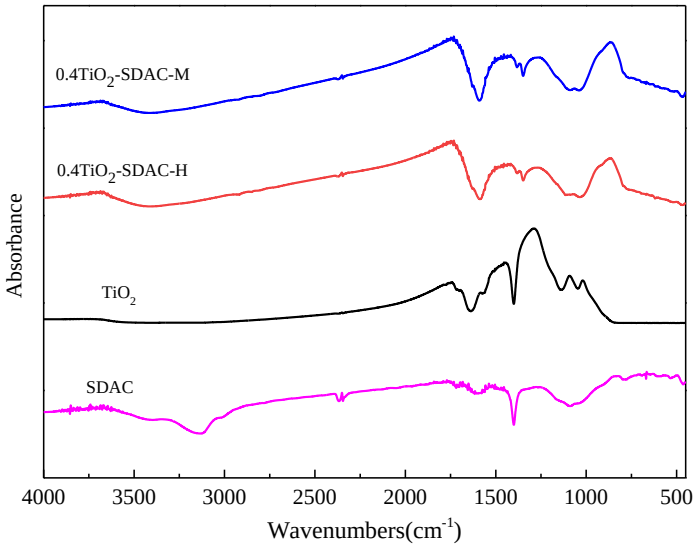

Figure 2. FTIR spectra of sludge-derived active carbon (SDAC), TiO_2, composite of 0.4TiO_2-SDAC-M prepared by physical mixing with mass ratio of 0.4 and composite of 0.4TiO_2-SDAC-H prepared by hydrothermal process for 4 h at 180°C.

Compared with 0.4TiO_2-SDAC-M, the dispersion of TiO_2 nanoparticles on the SDAC surface was better in 0.4TiO_2-SDAC-H. The high-temperature effect in the hydrothermal process may promote

the interaction relationship between TiO_2 nanoparticles and SDAC, which was conducive to forming of uniform TiO_2-SDAC composites.

To analyze the surface functional groups of the samples, FTIR spectra of SDAC, TiO_2, 0.4TiO_2-SDAC-M and 0.4TiO_2-SDAC-H were detected. As shown in Figure 2, the peaks in 0.4TiO_2-SDAC-M and 0.4TiO_2-SDAC-H were the same, which suggested that different synthesis methods had no noticeable effect on the functional group of the products. The peaks near 1600 cm^{-1} in both 0.4TiO_2-SDAC-M and 0.4TiO_2-SDAC-H indicated the presence of C=O and C=C bonds on the surface of TiO_2-SDAC composites [28, 29]. In SDAC, the peak around 1400 cm^{-1} caused by the bending vibration of hydroxyl groups. When combined with TiO_2, the vibration peak position of the O-H bond shifted to 1350 cm^{-1} and 1387 cm^{-1}. C-O stretching vibration can be detected at about 1043 and 1095 cm^{-1}.

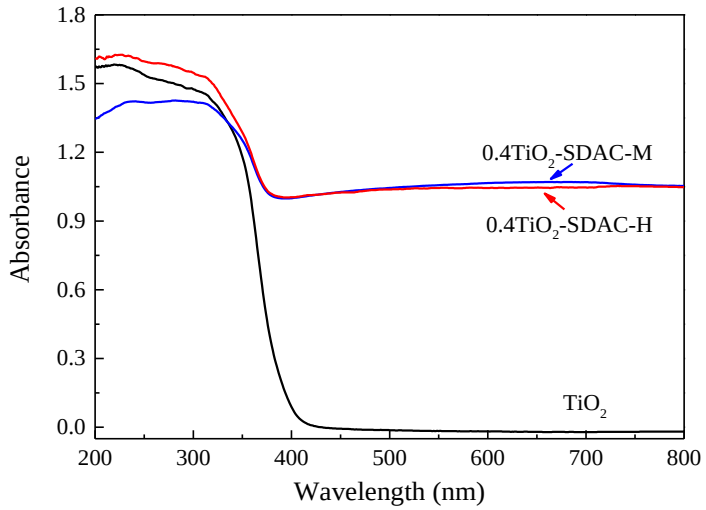

Figure 3. UV-Vis diffuse reflectance spectra of TiO_2, composite of 0.4TiO_2-SDAC-M prepared by physical mixing with mass ratio of 0.4 and composite of 0.4TiO_2-SDAC-H prepared by hydrothermal process for 4 h at 180°C.

UV-Vis diffuse reflectance absorption spectroscopy was used to evaluate the absorbance of the samples. As shown in Fig. 3, all samples had prominent absorption properties in the UV region (200-400 nm). However, there were apparent differences in the properties of the samples in the visible and near-infrared regions (400-800 nm). Compared with TiO_2, the absorbance of 0.4TiO_2-SDAC-M and 0.4TiO_2-SDAC-H gradually increased significantly. The introduction of SDAC can improve the absorbance of TiO_2, which may be due to the change of the electronic structure of TiO_2. After compounding with SDAC, the band gap energy of TiO_2 was reduced, and the sensitivity of TiO2 in the visible light range was improved [28]. The result also suggested that the synthetic method had little effect on the absorbance.

The chemical state of surface elements was investigated using X-photoelectron spectroscopy (XPS). In the full XPS survey spectra, C, O and Ti can be detected on the surface of TiO_2, 0.4TiO_2-SDAC-M and 0.4TiO_2-SDAC-H (Fig. 4a). Only one peak centered at about 284.8 eV can be seen in high-resolution C 1s spectra of all samples (Fig. 4b). Due to the presence of SDAC, the characteristic

peaks of C element can be detected in 0.4TiO_2-SDAC-M and 0.4TiO_2-SDAC-H. The C element in TiO_2 may come from CO_2 adsorbed in the air. For TiO_2, the peaks of Ti $2p_{3/2}$ and Ti $2p_{1/2}$ in high-resolution Ti 2p spectra were at 459.1 and 465.0 eV, which were characteristics of the Ti-O bond (Fig. 4c) [30]. After compounding with SDAC, the peak of Ti $2p_{3/2}$ shifted to higher binding energies of 459.5eV. For 0.4TiO_2-SDAC-H, the peak of Ti $2p_{1/2}$ can divide into two peaks, one of them remained at 465.0 eV, and the other shifted to higher binding energies of 465.5 eV.

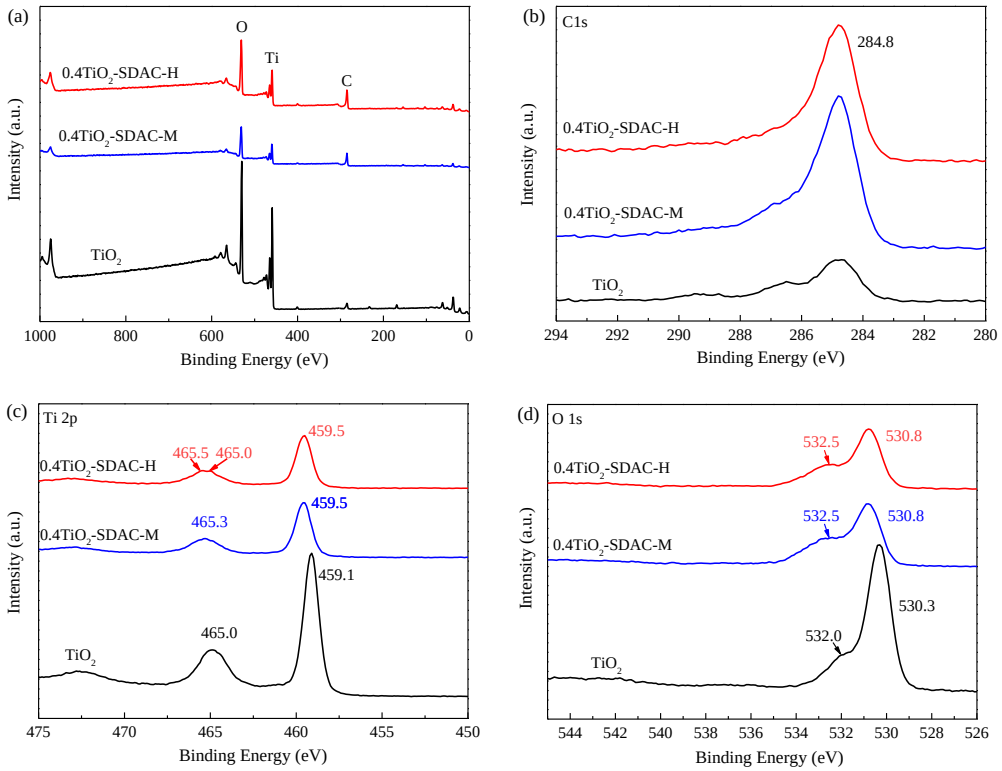

Figure 4. (a) XPS survey spectra, (b) C 1s, (c) Ti 2p and (d) O 1s core-level XPS spectra of TiO_2, composite of 0.4TiO_2-SDAC-M prepared by physical mixing with mass ratio of 0.4 and composite of 0.4TiO_2-SDAC-H prepared by hydrothermal process for 4 h at 180°C.

The shift may be caused by the substitution of O in part of TiO_2 by C to form a Ti-C bond [31]. The change of the Ti $2p_{1/2}$ peak can also be detected in 0.4TiO_2-SDAC-M, which indicates that the formation of the Ti-C bond also occurred in the process of physical mixing. Compared to the physical mixing approach, the hydrothermal method may give more incredible activation energy for the creation of chemical bonds and strengthen the development of the Ti-C bonds. For both 0.4TiO_2-SDAC-M and 0.4TiO_2-SDAC-H, the peaks of O 1s shifted to higher binding energies of 530.8 eV, meaning that the charge distribution around Ti and O in TiO_2 changed by compounding with SDAC (Fig. 4d).

Textural properties of TiO_2, SDAC and 0.4TiO_2-SDAC-H, were detected by N_2 adsorption isotherm (Table S1). The specific surface area of TiO_2, SDAC and 0.4TiO_2-SDAC-H were 80.13, 549.72 and 346.86 m^2/g, respectively. Compared with SDAC, the specific surface area of 0.4TiO_2-SDAC-H

decreased. It may be because the addition of titanium oxide nanoparticles reduced the average specific surface area and blocked the pores of SDAC [32].

3.2 Photocatalytic degradation of methylene blue

In the process of hydrothermal, the adsorption and photocatalytic properties of TiO_2-SDAC were affected by the reaction conditions. As shown in Fig. S2 and S3, the effects of reaction temperature and time on the adsorption and photocatalytic properties of $0.4TiO_2$-SDAC-H were not apparent. After optimization, the temperature of 180°C and the time of 4 h were chosen as the reaction conditions to synthesize $nTiO_2$-SDAC-H. The adsorption capacity and photocatalytic performance of TiO_2-SDAC prepared by physical mixing and hydrothermal process with the same mass ratio of TiO_2 to SDAC were compared in Fig. 5.

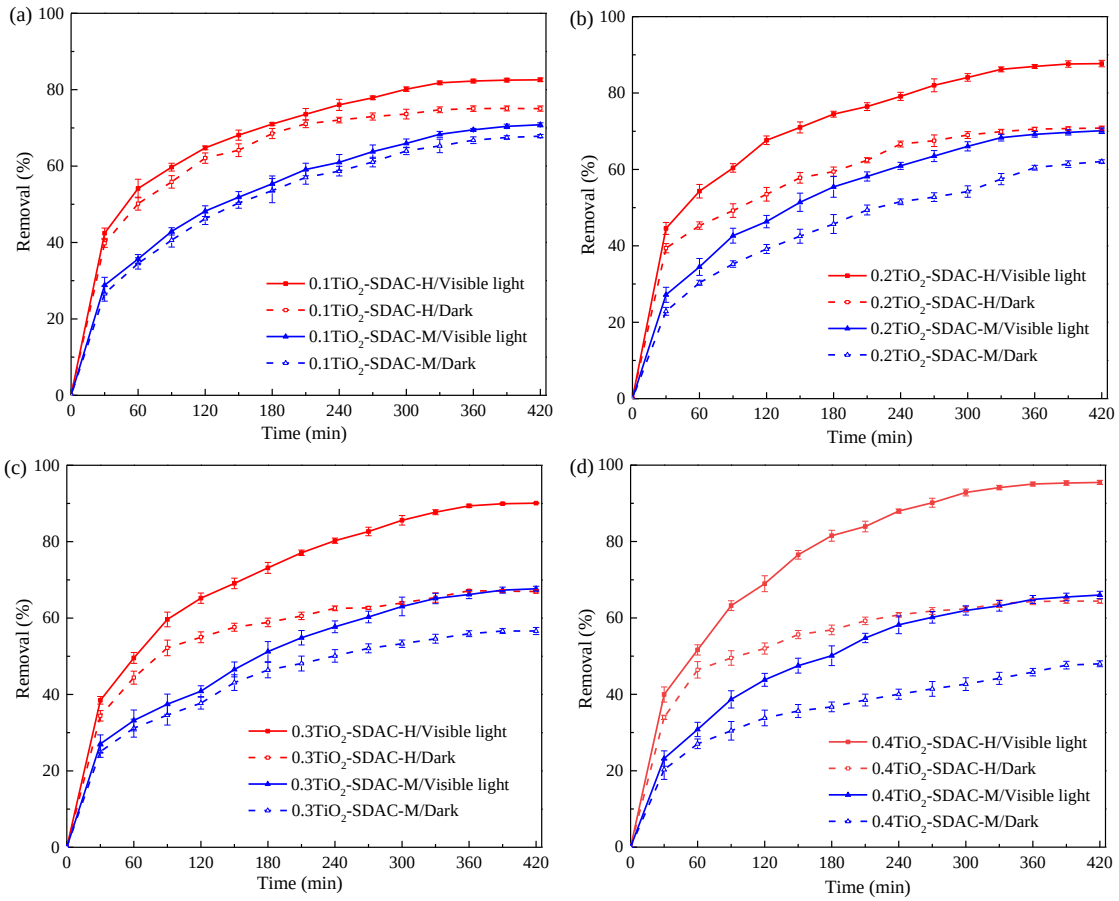

Figure 5. Removal of methylene blue (MB) under dark and visible light conditions, with TiO_2 to sludge-derived active carbon (SDAC) mass ratio of (a) 0.1, (b) 0.2, (c) 0.3 and (d) 0.4 by composite of TiO_2-SDAC-M prepared by physical mixing and composite of TiO_2-SDAC-H prepared by hydrothermal process for 4 h at 180°C.

In the dark condition, the removal of MB by TiO_2-SDAC-H prepared by the hydrothermal method was higher than that of TiO_2-SDAC-M. SDAC had a large specific surface area and pore volume, which determined the adsorption capacity of TiO_2-SDAC. When the content of TiO_2 in the system was the same, the difference in removal may be caused by the different interaction relationships between TiO_2 and SDAC. Compared with hydrothermal treatment, TiO_2 was more likely to occupy the pores of SDAC in the process of physical mixing. With an increase in TiO_2 mass, more adsorption sites were occupied, resulting in reduced removal. The removal of MB by TiO_2-SDAC increased under visible light, indicating that the addition of SDAC was conducive to improving the visible light photocatalytic performance of TiO_2. At the same time, the photocatalytic activity of TiO_2-SDAC increased with the increase of TiO_2 mass in the system. Both $0.4TiO_2$-SDAC-H and $0.4TiO_2$-SDAC-M showed better photocatalytic degradation performance under visible light. The addition of SDAC might change the electronic structure of TiO_2 and improve its photocatalytic performance under visible light. The photocatalytic performance of TiO_2-SDAC-H was better than that of TiO_2-SDAC-M, indicating that hydrothermal treatment with high temperature was more conducive to improving the photocatalytic performance of the composites.

Table 1. The degradation of methylene blue by the composites in the literatures.

Composite*	Light source	Maximum degradation (mg methylene blue / g composite)	Reference
(Yb, N)-TiO_2	Fluorescent lamp of 30 W	3.118	[33]
TiO_2 with graphene oxide	Xenon lamp of 500 W	9.900	[29]
low-cost carbon-modified TiO_2	OSRAM L 36 W/954 2G11 lamp	18.000	[34]
TiO_2/activated carbon	Mercury lamp	49.715	[32]
Immobilized Carbon-doped TiO_2 in Polyamide Fibers	Halogen lamps of 70 W	0.003	[28]
TiO_2/C composites	UV lamp of 15 W	7.028	[35]
Solvothermal carbon-doped TiO_2 photocatalyst	Sodium lamp with 99% visible light	0.050	[36]
$0.4TiO_2$-SDAC-H	Xenon lamp of 500 W	114.576	This work

* $0.4TiO_2$-SDAC-H was prepared by hydrothermal process for 4 h at 180°C, and the mass ratio of TiO_2 to SDAC was 0.4.

For TiO_2 modified by the physical mixing, the maximum removal of MB was 70.13%. In comparison, the MB removal of TiO_2 modified by the hydrothermal method can reach 95.48%. The degradation of MB by TiO_2-SDAC was also compared with those of TiO_2-AC composites presented in the related literature (Table 1). The maximum degradation of MB was used as evaluation index, which can be derived from the mass of MB degraded by per gram catalyst. It was shown that the maximum degradation by TiO_2-AC composite was lower than 50 mg methylene blue / g composite. However, the maximum degradation by TiO_2-SDAC was up to 114.576 mg methylene blue / g composite in this work.

3.3 Adsorption kinetics

In order to determine the adsorption rate of TiO_2-SDAC, the commonly used pseudo-first-order kinetic model was applied to simulate the experimental data and obtain the adsorption rate constant (k_{ads}, min^{-1}) [37],

$$\frac{dC_t}{d_t} = k_{ads}(C_e - C_t) \quad (1)$$

where C_e (mg L^{-1}) and C_t (mg L^{-1}) were the MB concentrations at equilibrium and time t (min), respectively.

Table 2. Adsorption fitting parameters of TiO_2 and sludge-derived active carbon (SDAC) composite under dark condition.

Method	Sample*	Parameters	
		k_{ads} (min^{-1})	R^2
Physical mixing	0.1TiO_2-SDAC-M	0.009	0.976
	0.2TiO_2-SDAC-M	0.008	0.962
	0.3TiO_2-SDAC-M	0.010	0.967
	0.4TiO_2-SDAC-M	0.011	0.951
Hydrothermal method	0.1TiO_2-SDAC-H	0.018	0.975
	0.2TiO_2-SDAC-H	0.015	0.938
	0.3TiO_2-SDAC-H	0.019	0.974
	0.4TiO_2-SDAC-H	0.020	0.968

* TiO_2-SDAC-M was prepared by physical mixing and TiO_2-SDAC-H was prepared by hydrothermal process for 4 h at 180°C, and the mass ratios of TiO_2 to SDAC were 0.1, 0.2, 0.3 and 0.4.

The effect of the synthesized method on the adsorption of MB by SDAC was displayed in Fig. 6. The MB adsorption was fitted well by pseudo-first-order kinetics with R^2 above 0.938. The maximum k_{ads} of 0.4TiO_2-SDAC-M and 0.4TiO_2-SDAC-H were 0.011 and 0.020 min^{-1}, respectively (Table 2). It was reported that adsorption of dye by activated carbon can also be fitted well with pseudo-first-order kinetics. The k_{ads} of Rhodamine B and Remazol Brillant Blue R by activated carbon prepared from wood chips and sewage sludge were 0.010 and 0.144 min^{-1}, respectively [25, 38]. The values of k_{ads} were similar to those of TiO_2-SDAC composite in this work. It suggested that introducing TiO_2 into the composite had no significant effect on the adsorption property of MB. The adsorption rate of TiO_2-

SDAC synthesized by the hydrothermal method was greater than that of physical mixing. During physical mixing, the MB molecule and TiO_2 nanoparticle in solution competed for the active site of SDAC, resulting in a decrease of adsorption rate. The adsorption rate was not significantly influenced by the changes of TiO_2 to SDAC mass ratio. It was reported that adsorption of methyl orange dye by TiO_2-SDAC composite can also be fitted well with pseudo-first-order kinetics. The k_{ads} of methyl orange was 0.023 min^{-1}, which was similar with that of MB in this work [39].

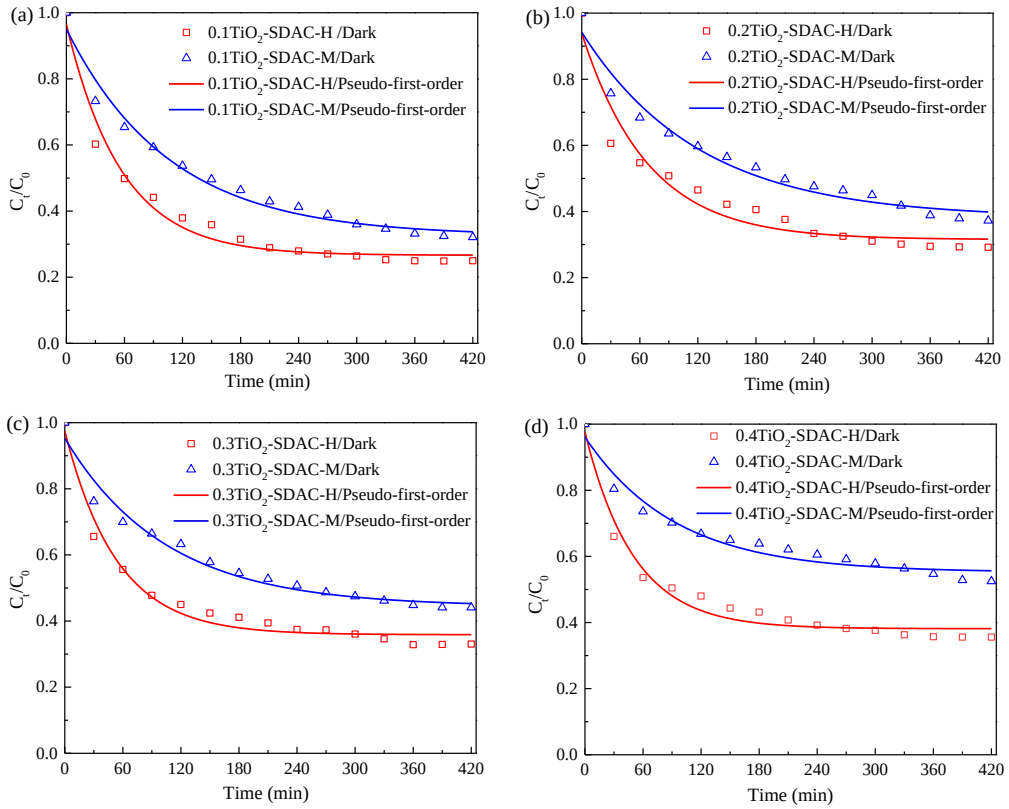

Figure 6. The fitting curves of pseudo-first-order kinetics under dark condition. TiO_2-SDAC-M was prepared by physical mixing and TiO_2-SDAC-H was prepared by hydrothermal process for 4 h at 180°C, and the mass ratios of TiO_2 to SDAC were 0.1, 0.2, 0.3 and 0.4.

3.4 Visible-light photocatalytic activity

Enhanced photocatalytic activity of TiO_2 has been achieved by surface modification. But here, we observed the enhanced photocatalytic activity of TiO_2 when mixed and loaded with SDAC. To estimate the photocatalytic activity of TiO_2-SDAC under visible light irradiation, the Elovich model was applied to simulate the removal kinetics of MB by TiO_2-SDAC synthesized by physical mixing and hydrothermal method [37]. The governing equation can describe as follow.

$$\frac{dC_t}{d_t} = - k_e C_0 e^{(\beta(C_t - C_0))} \qquad (2)$$

where k_e (min^{-1}) was the degradation rate constant, C_0 (mg L^{-1}) was the initial concentration, C_t (mg L^{-1}) was the concentration at the time of t (min), and β was a constant.

The experiment data of MB degradation was fitted well by the Elovich model with R^2 values larger than 0.988 (Table 3). The Elovich model was a heterogeneous model controlled by multiple processes. When photocatalysts such as TiO_2-SDAC were applied for MB removal visible light irradiation, both adsorption and photodegradation processes can be critical to the removal kinetics.

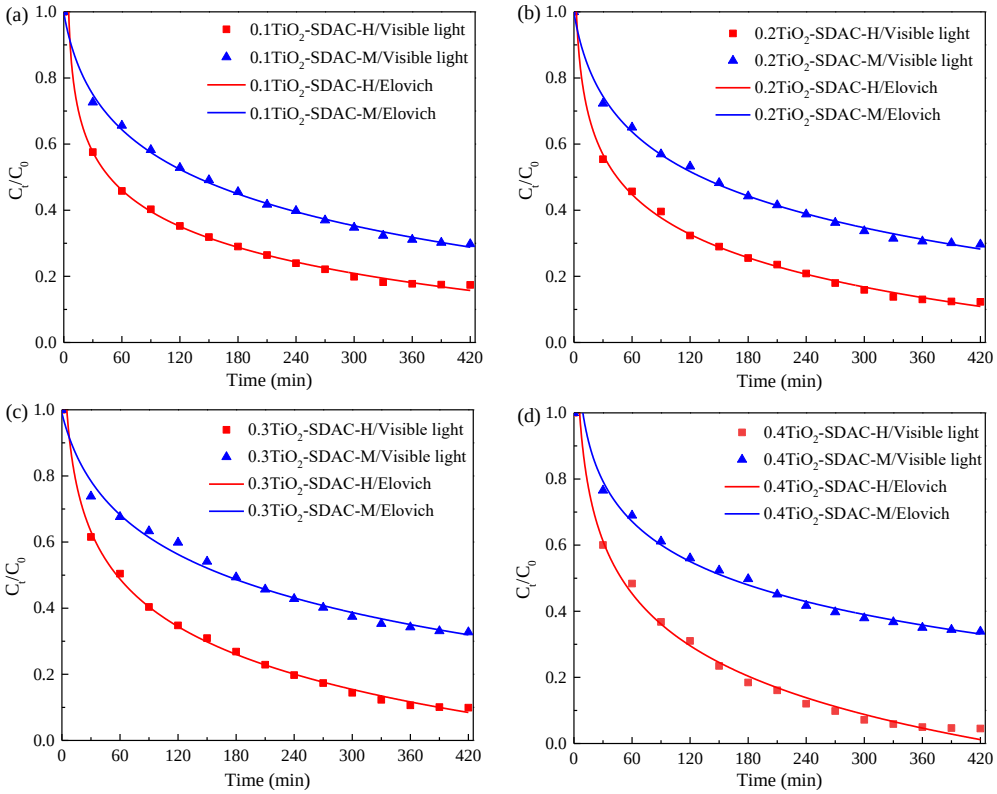

Figure 7. Kinetics fitting curves of MB degradation under visible light condition. TiO_2-SDAC-M was prepared by physical mixing and TiO_2-SDAC-H was prepared by hydrothermal process for 4 h at 180°C, and the mass ratios of TiO_2 to SDAC were 0.1, 0.2, 0.3 and 0.4.

For TiO_2-SDAC synthesized by the hydrothermal method, k_e increased from 0.742 to 1.121 min^{-1} along with an increase of TiO_2 to SDAC mass ratio (Table 3). It suggested that the removal rate of MB accelerated with an increase of TiO_2 mass during the hydrothermal process (Fig. 7). However, for physical mixing, k_e decreased along with the increased mass ratio of TiO_2 to SDAC. When the mass ratio was 0.4, the k_e of hydrothermal synthetic TiO_2-SDAC quadrupled that of physical mixing. Both physical mixing and hydrothermal method tended to enhance the photocatalytic degradation of MB. It was reported that k_e of TiO_2-SDAC synthesized by physical mixing can be up to 0.537 min^{-1} under pure visible light, which was still lower than that of hydrothermal synthetic TiO_2-SDAC [27]. Although

physical mixing was low energy consumption and minimized environmental pollution, TiO_2-SDAC synthesized by the hydrothermal method exhibited higher photocatalytic performance under visible light.

Two reasons may account for the high visible-light activity of TiO_2 modified by SDAC. First, SDAC with a high surface area can provide large amounts of active sites and adsorb the most reactive species, improving mass transfer between TiO_2 and MB in solution. Second, it was considered that the carbon atoms were introduced into the TiO_2 lattice. TiO_2-SDAC can adsorb visible light and generate electron/hole pairs, followed by their reaction with oxygen and H_2O to generate hydroxyl radicals (•OH) and superoxide ion radicals ($O_2^{\bullet-}$). Finally, the resulting functional radicals were capable of degrading MB (Fig. S4). Besides TiO_2-SDAC, TiO_2/carbon nanotube and TiO_2/graphene were two kinds of TiO_2/carbon-based materials. The photocatalytic performance of TiO_2/carbon nanotube was 2.5 times more than that of TiO_2 for MB degradation [40-42]. Carbon nanotubes prevented TiO_2 nanoparticles from aggregating by providing sufficient sites. High dispersion of TiO_2/carbon nanotube led to higher photocatalytic activity. The main drawback was the blocking of the irradiation by carbon nanotube, which reduced the production of the radicals and decreased the photocatalytic activity. The photocatalytic performance of TiO_2/graphene was 15 times more than that of TiO_2 [43-45]. High conductivity of graphene was beneficial to capture photogenerated electrons and promote charge transfer to produce free radicals[46, 47]. The main disadvantage was that graphene mask the photocatalysts when coupled at higher percentages and decreases the photocatalysis. The main disadvantage of TiO_2-SDAC was also the blocking of the irradiation. However, the surface area of TiO_2-SDAC was higher than TiO_2/carbon nanotube and TiO_2/graphene. It was suggested that a large number of free radicals and active sites produced on the surface of the composite, resulted in higher photocatalytic activity.

Table 3. Kinetics parameters of Elovich model.

Method	Sample*	Parameters		
		k_e (min^{-1})	β	R^2
Physical mixing	0.1TiO_2-SDAC-M	0.394	0.126	0.995
	0.2TiO_2-SDAC-M	0.399	0.124	0.997
	0.3TiO_2-SDAC-M	0.307	0.117	0.988
	0.4TiO_2-SDAC-M	0.275	0.140	0.989
Hydrothermal method	0.1TiO_2-SDAC-H	0.742	0.166	0.996
	0.2TiO_2-SDAC-H	0.893	0.140	0.994
	0.3TiO_2-SDAC-H	0.963	0.119	0.995
	0.4TiO_2-SDAC-H	1.121	0.111	0.988

* TiO_2-SDAC-M was prepared by physical mixing and TiO_2-SDAC-H was prepared by hydrothermal process for 4 h at 180°C, and the mass ratios of TiO_2 to SDAC were 0.1, 0.2, 0.3 and 0.4.

4. CONCLUSIONS

Anatase TiO_2 was modified with SDAC through the physical mixing and hydrothermal method. XPS analysis showed the presence of a Ti-C bond. Under visible light irradiation, the removal of MB with a concentration of 40 mg L^{-1} by TiO_2-SDAC synthesized through the physical mixing and hydrothermal method were up to 70.13% and 95.48%, respectively. Experimental results indicated that

the pseudo-first-order kinetic fitted well with adsorption data. The Elovich model worked well with visible-light photocatalytic data. Both physical mixing and hydrothermal synthesis tended to enhance the photocatalytic degradation of MB. Compared with physical mixing, hydrothermal synthetic TiO_2-SDAC exhibits higher visible-light photocatalytic activity. As a result, SDAC can adsorb, support and enhance the photocatalytic activity of TiO_2.

ACKNOWLEDGEMENTS
This work was supported by the Fundamental Research Funds for Colleges and Universities in Liaoning Province, China (grant number lnjc202012 and lnqn202020).

SUPPORTING MATERIAL

Preparation of TiO_2-sludge-derived activated carbon under different temperature and time in hydrothermal process

For hydrothermal process, hydrothermal temperature and time were also optimized. When the reaction time was 4 h, we selected 120, 150 and 180℃ as the reaction temperature to test the effect of temperature on the properties of the TiO_2-SDAC-H. Similarly, when the reaction temperature was 180 ℃, we selected 2, 4, 6 and 8 h as the reaction time for synthesis, and tested the effect of the reaction time on the properties of TiO_2-SDAC-H.

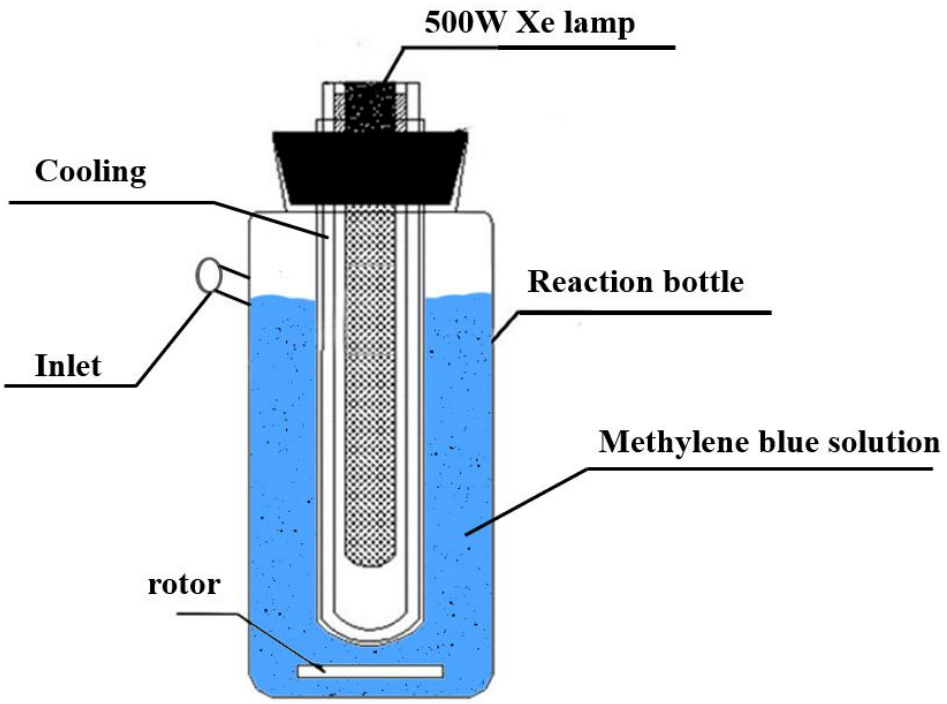

Fig. S1 The equipment diagram of photocatalytic degradation experiment.

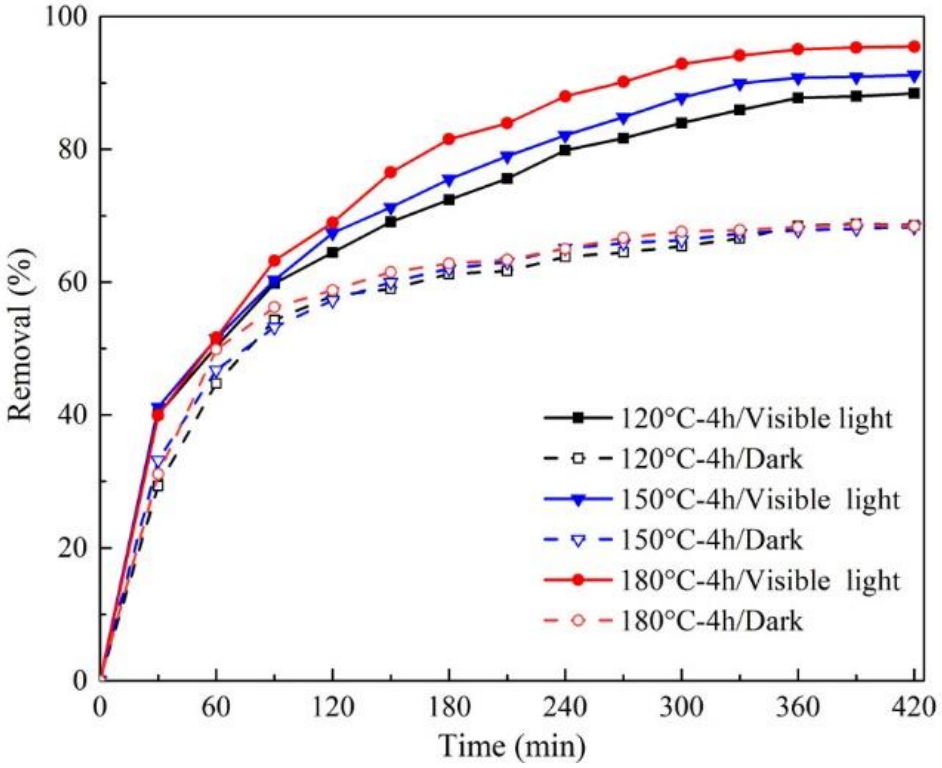

Fig. S2 Removal of methylene blue (MB) by composite under dark and visible light condition. The composite was prepared by hydrothermal process for 4 h at different temperatures.

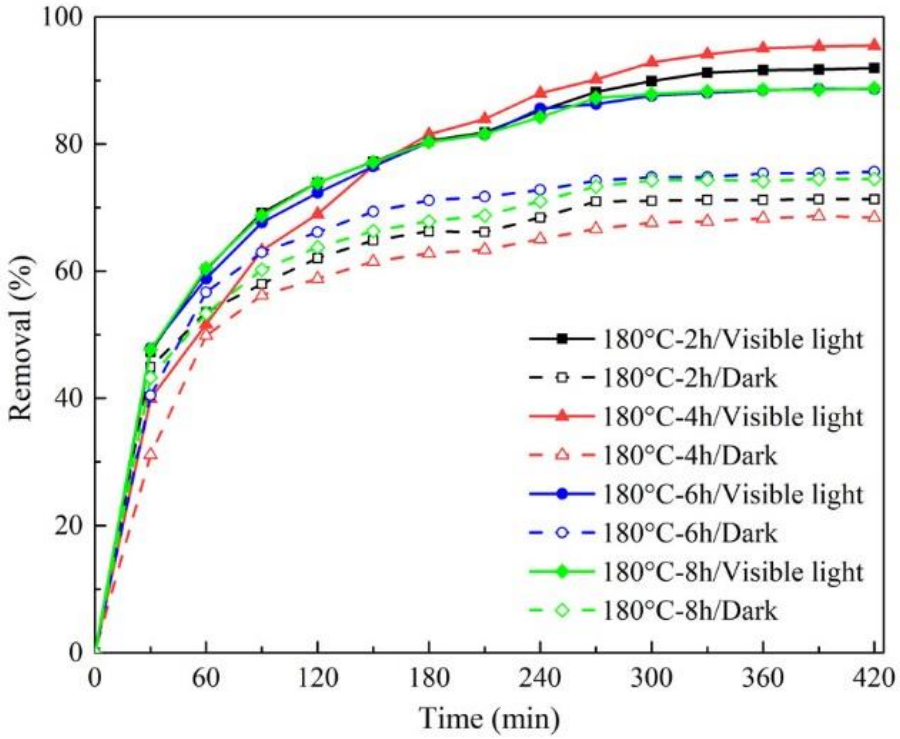

Fig. S3 Removal of methylene blue (MB) by composite under dark and visible light condition. The composite was prepared by hydrothermal process with the temperature of 180 °C at different hydrothermal times.

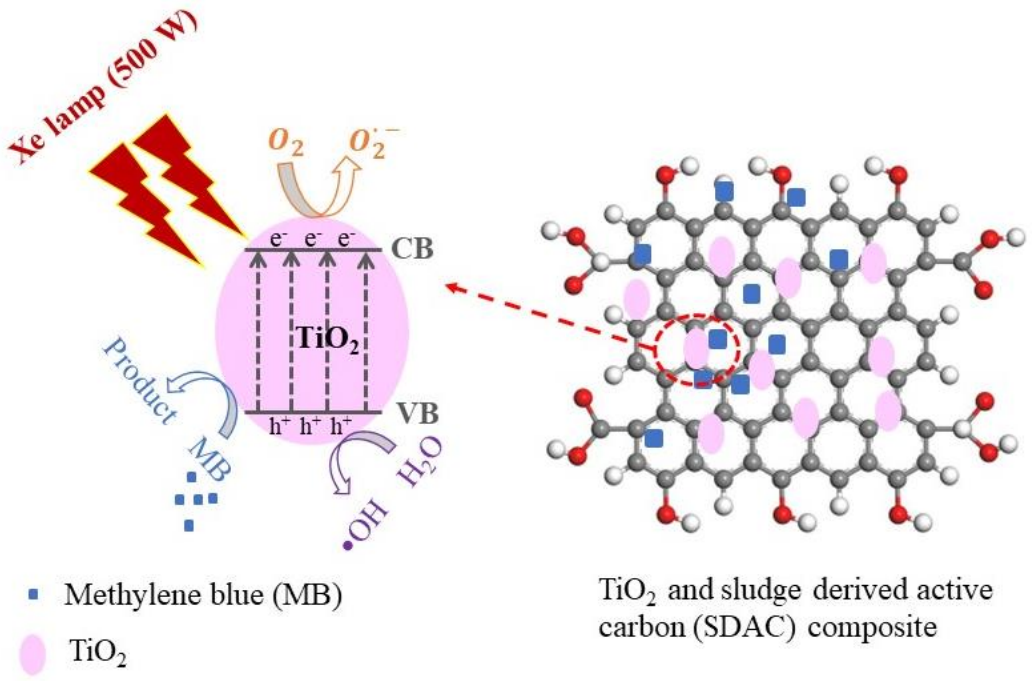

Fig. S4 Proposed mechanism of MB photocatalytic degradation process on composite.

Table S1 Specific surface area and pore structure of TiO_2, sludge-derived active carbon (SDAC) and composite.

Samples*	Specific surface area （m^2/g）	Total pore volume （cm3/g）
TiO_2	82.13	0.30
SDAC	549.72	0.37
0.4TiO_2-SDAC-H	346.86	0.33

* 0.4TiO_2-SDAC-H was prepared by hydrothermal process for 4 h at 180°C, and the mass ratio of TiO_2 to SDAC was 0.4.

References

1. A. Gopinath, G. Divyapriya, V. Srivastava, A.R. Laiju, P.V. Nidheesh and M.S. Kumar, *Environ. Res.*, 194 (2021) 110656.
2. M. Schnell, T. Horst and P. Quicker, *J. Environ. Manage.*, 263 (2020) 110367.
3. K. Gong, Q. Hu, L. Yao, M. Li, D. Sun, Q. Shao, B. Qiu and Z. Guo, *ACS Sustain. Chem. Eng.*, 6 (2018) 7283.
4. W. Hu, W. Tong, Y. Li, Y. Xie, Y. Chen, Z. Wen, S. Feng, X. Wang, P. Li, Y. Wang and Y. Zhang, *J. Hazard. Mater.*, 388 (2020) 121801.
5. P. Hadi, M. Xu, C. Ning, C. Sze Ki Lin and G. McKay, *Chem. Eng. J.*, 260 (2015) 895.
6. T.S. Hui and M.A.A. Zaini, *Biomass Convers. Biorefin.*, 12 (2022) 2847.
7. M.F. Chowdhury, S. Khandaker, F. Sarker, A. Islam, M.T. Rahman and M.R. Awual, *J. Mol. Liq.*, 318 (2020) 114061.

8. C.J. Li, Y.J. Zhang, H. Chen, P.Y. He and Q. Meng, *J. Clean. Prod*., 348 (2022) 131278.
9. W. Li, B. Mu and Y. Yang, *Bioresour. Technol*., 277 (2019) 157.
10. P. Senthil Kumar, S.J. Varjani and S. Suganya, *Bioresour. Technol*., 250 (2018) 716.
11. Q. Li, T. Zhao, M. Li, W. Li, B. Yang, D. Qin, K. Lv, X. Wang, L. Wu, X. Wu and J. Sun, *Appl. Catal. B: Environ.*, 249 (2019) 1.
12. C.H. Nguyen, C.-C. Fu and R.-S. Juang, *J. Clean. Prod*., 202 (2018) 413.
13. K. Venkatesh, G. Arthanareeswaran, A.C. Bose and P.S. Kumar, *Sep. Purif. Technol*., 241 (2020) 116709.
14. T. Fazal, A. Razzaq, F. Javed, A. Hafeez, N. Rashid, U.S. Amjad, M.S. Ur Rehman, A. Faisal and F. Rehman, *J. Hazard. Mater*., 390 (2020) 121623.
15. X. Liu, Y. Liu, S. Lu, W. Guo and B. Xi, *Chem. Eng. J*., 350 (2018) 131.
16. N.G. Sagharloo, M. Rabani, L. Salimi, H. Ghafourian and S.M.T. Sadatipour, *Biomass Convers. Biorefin.*, (2021).
17. W. Ren, Z. Ai, F. Jia, L. Zhang, X. Fan and Z. Zou, *Appl. Catal. B: Environ*., 69 (2007) 138.
18. L. Wang, J. Guo, J. Dang, X. Huang, S. Chen and W. Guan, *Water Sci. Technol*., 78 (2018) 1082.
19. W.-H. Li, Q.-Y. Yue, B.-Y. Gao, Z.-H. Ma, Y.-J. Li and H.-X. Zhao, *Chem. Eng. J.*, 171 (2011) 320.
20. R. Leary and A. Westwood, *Carbon*, 49 (2011) 741.
21. M.M. Mian and G. Liu, *Chemosphere*, 215 (2019) 101.
22. S. Krishnan, N.S. Zulkapli, M.F.B.M. Din, Z.A. Majid, M. Nasrullah and F.M. Sairan, *Biomass Convers. Biorefin*., (2021).
23. Y.L. Pang, S. Lim and R.K.L. Lee, *Environ. Sci. Pollut. Res*., 27 (2020) 34638.
24. T.-T. Lim, P.-S. Yap, M. Srinivasan and A.G. Fane, *Crit. Rev. Environ. Sci. Technol*., 41 (2011) 1173.
25. T.L. Silva, A. Ronix, O. Pezoti, L.S. Souza, P.K.T. Leandro, K.C. Bedin, K.K. Beltrame, A.L. Cazetta and V.C. Almeida, *Chem. Eng. J*., 303 (2016) 467.
26. E. Shi, X. Wang, M. Zhang, X. Wang, J. Gao and Y. Zheng, *Environ. Chem. Lett*., (2022).
27. J. Matos, M. Rosales, A. García, C. Nieto-Delgado and J.R. Rangel-Mendez, *Green Chem*., 13 (2011) 3431.
28. S.N.B. Saiful Amran, V. Wongso, N.S. Abdul Halim, M.K. Husni, N.S. Sambudi and M.D.H. Wirzal, *J. Asian Ceram. Soc*., 7 (2019) 321.
29. T.A. Kurniawan, Z. Mengting, D. Fu, S.K. Yeap, M.H.D. Othman, R. Avtar and T. Ouyang, *J. Environ. Manage.*, 270 (2020) 110871.
30. Y.-x. Zhao, X.-y. Li, C. Tian and J.-x. Wang, *J. Clean. Prod*., 267 (2020) 121979.
31. R. Huo, J.-Y. Yang, Y.-Q. Liu, H.-F. Liu, X. Li and Y.-H. Xu, *Mater. Res. Bull*., 76 (2016) 72.
32. W. Xu, Y. Jin, Y. Ren, J. Li, Z. Wei, C. Ban, H. Cai and M. Chen, *Can. J. Chem. Eng*., 100 (2022) 276.
33. J. Zhang, L.J. Xu, Z.Q. Zhu and Q.J. Liu, *Mater. Res. Bull*., 70 (2015) 358.
34. N.P. de Moraes, M.L.C.P. da Silva, T.M.B. Campos, G.P. Thim and L.A. Rodrigues, *J. Sol-Gel Sci. Technol.*, 87 (2018) 380.
35. J. Cai, S. Hu, J. Xiang, H. Zhang and D. Men, *RSC Adv*., 10 (2020) 40830.
36. J. Matos, A. García, L. Zhao and M.M. Titirici, *Appl. Catal. A: Gen*., 390 (2010) 175.
37. Y. Luo, X. Wei, B. Gao, W. Zou, Y. Zheng, Y. Yang, Y. Zhang, Q. Tong and L. Dong, *Chem. Eng. J.*, 375 (2019) 122019.
38. T. Maneerung, J. Liew, Y. Dai, S. Kawi, C. Chong and C.-H. Wang, *Bioresour. Technol*., 200 (2016) 350.
39. M.N. Rashed, M.A. Eltaher and A.N.A. Abdou, *R. Soc. Open Sci*., 4 (2017) 170834.
40. M. Shaban, A.M. Ashraf and M.R. Abukhadra, *Sci. Rep.*, 8 (2018) 781.
41. C.H. Park, C.M. Lee, J.W. Choi, G.C. Park and J. Joo, *Ceram. Int*., 44 (2018) 1641.
42. H.K. Sharma, S.K. Sharma, K. Vemula, A.R. Koirala, H.M. Yadav and B.P. Singh, *Solid State Sci*., 112 (2021) 106492.

43. N.N.T. Ton, A.T.N. Dao, K. Kato, T. Ikenaga, D.X. Trinh and T. Taniike, *Carbon*, 133 (2018) 109.
44. X. Liu, W. Yang, C. Yu and H. Zhang, *J. Environ. Chem. Eng*., 6 (2018) 4899.
45. H. Zhang, X. Lv, Y. Li, Y. Wang and J. Li, *ACS Nano*, 4 (2010) 380.
46. Y.H. Yao Fang, ZhiJiang Ni, ZhiLei Wang, Shifei Kang, Yangang Wang, Xi Li, *Int. J. Electrochem. Sci.*, 12 (2017) 5951.
47. W.Z. Tianyu Du, Han Peng, Gaurav Jain, *Int. J. Electrochem. Sci*., 13 (2018) 6229